Signature splitting and inversion in neutron-deficient $^{117-127}$Ba isotopes: a systematic total-Routhian-surface study*

Jie Yang (杨婕)[1] Qing-Zhen Chai (柴清祯)[2†] Hua-Lei Wang (王华磊)[3] Kui-Peng Li (李葵鹏)[1]

[1]Department of Physics, Liaoning Normal University, Dalian 116029, China
[2]School of Physics and Advanced Energy, Henan University of Technology, Zhengzhou 450001, China
[3]School of Physics, Zhengzhou University, Zhengzhou 450001, China

Abstract: Signature splitting in the $\nu h_{11/2}$ rotational bands of the odd-N neutron-deficient isotopes $^{117-127}$Ba is investigated systematically. Band crossings and shape evolution are studied using pairing- and deformation-self-consistent Woods-Saxon-Strutinsky calculations within the total-Routhian-surface (TRS) method in the (β_2,γ,β_4) deformation space. Calculated alignments and deformation-dependent Routhians indicate that proton-pair alignment is favored in $^{117-123}$Ba, whereas proton and neutron alignments compete in ^{125,127}Ba. The signature splitting of the lowest $h_{11/2}$ quasineutron Routhians is examined as a function of β_2 and γ, both below and above the first band crossing. The observed reduction and occasional inversion of the splitting are interpreted qualitatively in terms of competing γ-driving tendencies of the strongly coupled odd neutron and the aligned proton pair. For the heavier isotopes, the calculations associate large splitting with an aligned, oblate $\nu h_{11/2}$ configuration; this association may help explain why only one member of a partner pair has been identified experimentally at high spin.

Keywords: total-Routhian-surface calculations, signature splitting, quasiparticle alignment, shape coexistence, neutron-deficient nuclei

DOI: 10.1088/1674-1137/aea10b **CSTR:** 32044.14.ChinesePhysicsC.50114108

I. INTRODUCTION

Signature is a quantum number used to classify high-spin rotational spectra and is associated with the symmetry of the nuclear wave function under a rotation of 180° about an axis perpendicular to the symmetry axis [1]. For a deformed, rotating nucleus, signature distinguishes two energetically similar sequences of states that differ in angular momentum by one unit ($\Delta I = 1$) [2]. These sequences, known as signature-partner bands, are labeled by signature quantum numbers $\alpha = \pm 1/2$ for odd-mass nuclei and arise from the intrinsic symmetry of the single-particle orbitals under rotation. The energy difference between these partner bands, termed signature splitting, is sensitive to shell structure, deformation, and rotational frequency, making it a useful probe of nuclear shape and quasiparticle configurations [3].

The origin of signature splitting is fundamentally linked to the admixture of $K = 1/2$ components in the quasiparticle wave functions. Thus, signature splitting serves as a sensitive indicator of two-quasiparticle bands and provides insight into the deformation-driving effects of the orbitals involved in their coupling [4–6]. Large signature splitting is generally observed for low-K orbitals within a high-j shell, whereas mid- to high-K orbitals exhibit smaller splitting owing to reduced $K = 1/2$ admixture [7, 8]. The splitting is sensitive to nuclear triaxiality, as different quasiparticles can induce different γ deformation values depending on the position of the chemical potential [9].

Signature inversion, a reversal of the usual signature splitting pattern at low spin, has been observed in odd-odd nuclei where both odd nucleons occupy high-j orbitals, such as the $\pi h_{11/2} \otimes \nu h_{11/2}$ configuration near $A \approx 130$ and the $\pi h_{11/2} \otimes \nu i_{13/2}$ configuration near $A \approx 160$ [5, 6]. Theoretical interpretations of signature inversion invoke beyond-mean-field effects, including dynamic deformations associated with vibrations [10], wobbling motion [11], proton-neutron residual interactions [12], and quadrupole pairing correlations [6]. This pronounced phenomenon is a valuable indicator of triaxiality in rotating γ-soft nuclei [13].

The odd-A barium isotopes $^{117-127}$Ba lie between the neutron shell closures at $N = 50$ and $N = 82$. This mass region is of particular interest because it exhibits large quadrupole deformations (β_2), with the neutron Fermi

Received 15 July 2026; Accepted 1 September 2026; Accepted manuscript online 2 September 2026

* Supported by the National Natural Science Foundation of China (Nos. 203070092510, 12205076), the General Program of Natural Science Foundation of Henan Province (No. 262300420311), and the Cultivation Programme for Young Backbone Teachers in Henan University of Technology (No. 21421304)

† E-mail: E-mail: chaiqz@haut.edu.cn

©2026 Chinese Physical Society and the Institute of High Energy Physics of the Chinese Academy of Sciences and the Institute of Modern Physics of the Chinese Academy of Sciences and IOP Publishing Ltd. All rights, including for text and data mining, AI training, and similar technologies, are reserved.

surface near the middle of the $\nu h_{11/2}$ shell and the proton Fermi surface in the lower part of the intruder subshell. Consequently, proton and neutron excitations compete and drive the nuclear shape toward prolate and oblate configurations, respectively [14].

The odd-N nuclei are particularly useful for studying proton alignment because the odd neutron blocks one member of the lowest neutron-pair alignment. Previous calculations have demonstrated that the relative proton and neutron alignment frequencies are sensitive to nuclear shape [15, 16]. At low frequency, the shape of these γ-soft nuclei is strongly influenced by the valence quasineutron; at higher frequency, the deformation-driving effects of the aligned quasiparticles must also be included [17]. Observables such as signature splitting therefore provide a sensitive probe of the deformation and configuration of odd-A nuclei [3, 13, 18, 19]. However, a small signature splitting may also reflect tilted-axis rotation, which is beyond the present principal-axis framework [20].

This sensitivity is pronounced in the low-lying negative-parity bands of $^{117-127}$Ba. The one-quasiparticle bands below the first crossing and the three-quasiparticle bands above it need not have the same equilibrium deformation. The present work focuses on bands based on a neutron $h_{11/2}$ quasiparticle and follows the effects of proton and neutron $h_{11/2}$ pair alignments as the rotational frequency increases. Previous investigations reported substantial signature splitting in neutron $h_{11/2}$ bands with $K^\pi = 5/2^-$ or $7/2^-$ for nuclei with $N = 61-71$. These bands have been interpreted using, among other approaches, the interacting boson model [21, 22] and the projected shell model [23]. The present work adds a configuration-dependent, isotope-wide TRS analysis. In particular, it (i) compares the measured and calculated alignments for both signatures, (ii) tracks the β_2 and γ dependence of the lowest quasiparticle Routhians on both sides of the first crossing, and (iii) separates the proton-aligned and neutron-aligned interpretations of the high-spin bands in the heavier isotopes. This provides a unified test of how shape evolution and quasiparticle alignment control signature splitting across the $^{117-127}$Ba chain.

This paper is organized as follows. Section 2 elaborates on the fundamental principles and computational procedures of the present pairing- and deformation-self-consistent Woods-Saxon-Strutinsky calculations. Section 3 systematically presents the numerical results on signature splitting and inversion in $^{117-127}$Ba isotopes, together with an in-depth analysis and comparative discussion. Section 4 concludes by summarizing the main findings and key innovations of this study and outlines feasible directions and prospects for future work.

II. THE THEORETICAL FRAMEWORK

The total-Routhian-surface (TRS) calculations used in this work are based on a pairing- and deformation-self-consistent cranked mean-field approach [6, 24]. The total nuclear energy consists of a macroscopic component and a microscopic correction. The macroscopic energy is derived from the shape-dependent liquid-drop model (LDM), with parameters adopted from Myers and Swiatecki [25]. The microscopic correction, which reflects the nonuniform distribution of single-particle levels in the nucleus, primarily includes shell and pairing corrections. These are computed using the Strutinsky smoothing method [26] and the Lipkin-Nogami (LN) method [27, 28], respectively.

In the cranking approximation, the nucleus rotates about the fixed x axis at rotational frequency ω. Pairing correlations, which depend on both frequency and deformation, are treated within the cranked Hartree-Fock-Bogoliubov approximation. The equations are solved at each point on a deformation grid in (β_2,γ,β_4), and the pairing field is determined self-consistently at each frequency and deformation.

Approximate particle-number projection is included through the Lipkin-Nogami method. The resulting cranked Lipkin-Nogami equations define the quasiparticle Routhians [2, 24]. The auxiliary Routhian $\hat{\mathcal{H}}$ is

$$\hat{\mathcal{H}} = \hat{H}^\omega - \lambda_1\hat{N} - \lambda_2\hat{N}^2, \tag{1}$$

where $\hat{N}$ denotes the nucleon-number operator and $\hat{H}^\omega$ denotes the cranking Hamiltonian, which comprises the single-particle Hamiltonian $\hat{H}_{\rm sp}$, the pairing Hamiltonian $\hat{H}_{\rm pair}$, and the cranking term,

$$\hat{H}^\omega = \hat{H}_{\rm sp} + \hat{H}_{\rm pair} - \omega\hat{J}_x = \sum_k e_k a_k^\dagger a_k - G\sum_{k,l>0} a_k^\dagger a_{\bar{k}}^\dagger a_{\bar{l}} a_l - \omega\hat{J}_x, \tag{2}$$

where e_k denotes the single-particle energy, G is the pairing strength, and $|\bar{k}\rangle = \hat{T}|k\rangle$, where $\hat{T}$ is the time-reversal operator. The operator $\hat{J}_x$ is the x component of the total angular momentum, and $a^\dagger$ and a denote particle creation and annihilation operators, respectively. The monopole pairing strengths were determined separately for protons and neutrons using the average-gap prescription of Møller and Nix [29]. For each particle species $\tau = p,n$, the pairing strength is calculated as

$$G_\tau = \frac{2}{\widetilde{\rho}_\tau}\left[\ln\left(\frac{\sqrt{y_{2,\tau}^2+\bar{\Delta}_\tau^2}+y_{2,\tau}}{\sqrt{y_{1,\tau}^2+\bar{\Delta}_\tau^2}+y_{1,\tau}}\right)\right]^{-1}, \tag{3}$$

in which

$$y_{1,\tau} = \frac{-N_\tau/2+n_{1,\tau}-1}{\widetilde{\rho}_\tau}, y_{2,\tau} = \frac{-N_\tau/2+n_{2,\tau}}{\widetilde{\rho}_\tau}, \tag{4}$$

where $\widetilde{\rho}_\tau$ is the smoothed single-particle level density at the Fermi surface, and $n_{1,\tau}$ and $n_{2,\tau}$ define the pairing window. The empirical average pairing gap is used in [29]

$$\bar{\Delta}_\tau = 3.3 N_\tau^{-1/3} f_\tau \text{ MeV}. \tag{5}$$

In the Lipkin-Nogami method, the expectation value of $\hat{\mathcal{H}}$ is varied, with λ_1 and λ_2 treated as Lagrange multipliers:

$$\delta\langle\Phi|\hat{\mathcal{H}}|\Phi\rangle = 0, \tag{6}$$

where $|\Phi\rangle$ takes the standard BCS form

$$|\Phi\rangle = \prod_k (u_k + v_k a_k^\dagger a_{\bar{k}}^\dagger)|0\rangle, \tag{7}$$

with the normalisation condition

$$u_k^2 + v_k^2 = 1, \tag{8}$$

where $|0\rangle$ denotes the particle vacuum, and v_k^2 and u_k^2 are the occupation and vacancy probabilities, respectively. Thus, the self-consistent monopole pairing gap is

$$\Delta_\tau = G_\tau \sum_k u_{k\tau} v_{k\tau}. \tag{9}$$

The Lagrange multipliers λ_1 and λ_2, as well as the rotational frequency, are determined by constraining the particle number and the angular momentum along the rotational axis:

$$\langle\Phi|\hat{N}|\Phi\rangle = n, \quad n = Z \text{ or } N, \tag{10}$$

and

$$\langle\Phi|\hat{J}_x|\Phi\rangle = I_x. \tag{11}$$

Here, λ_1 constrains the mean particle number, whereas λ_2 is obtained from the auxiliary equation for particle-number fluctuations,

$$\lambda_2 = \frac{G}{4} \frac{\sum_{k>0}(u_k^3 v_k)\sum_{k>0}(u_k v_k^3) - \sum_{k>0}(u_k v_k)^4}{\sum_{k>0}(u_k^2 v_k^2)^2 - \sum_{k>0}(u_k v_k)^4}. \tag{12}$$

The microscopic Lipkin–Nogami gap corresponding to the experimental odd–even mass difference is defined as

$$\Delta_{\text{LN},\tau} = \Delta_\tau + \lambda_{2,\tau}, \qquad \tau = p, n. \tag{13}$$

The single-particle energies used in the shell correction are calculated using the deformed Woods-Saxon (WS) potential and its universal parametrization [30]. The WS Hamiltonian is diagonalized in an oscillator basis including shells up to $N_{\text{osc}} = 12$ for protons and $N_{\text{osc}} = 14$ for neutrons.

The nuclear surface is parameterized by a spherical-harmonic expansion [31]. In the Lund convention [32], the Cartesian quadrupole coordinates are

$$X = \beta_2 \cos(\gamma + 30^\circ) \quad \text{and} \quad Y = \beta_2 \sin(\gamma + 30^\circ). \tag{14}$$

The γ parameter ranges from -120° to 60°. This range can be divided into three sectors, $-120^\circ < \gamma < -60^\circ$, $-60^\circ < \gamma < 0^\circ$, and $0^\circ < \gamma < 60^\circ$, which correspond to the same triaxial shapes at zero frequency but to rotation about the long, medium, and short axes, respectively, at nonzero cranking frequency. The four limiting values of γ at -120°, -60°, 0°, and 60° correspond to axially symmetric shapes exhibiting different rotational behaviors. In particular, $\gamma = -120^\circ$ and 0° correspond to prolate shapes, whereas $\gamma = \pm 60^\circ$ correspond to oblate shapes, each with a distinct orientation of the nuclear symmetry axis relative to the rotation axis. At $\gamma = -120^\circ$ and 60°, the nucleus undergoes non-collective rotation about its symmetry axis, whereas at $\gamma = -60^\circ$ and 0°, the rotation is collective and occurs about an axis perpendicular to the symmetry axis.

In reflection-symmetric nuclei, both signature (r) and intrinsic parity (π) are good quantum numbers. The signature quantum number r is the eigenvalue of the operator $\hat{\mathcal{R}}_x = \exp(-i\pi\hat{J}_x)$. It is conventionally written as [1, 2]

$$r = e^{-i\pi\alpha}. \tag{15}$$

For a state of spin I, this gives

$$r = e^{-i\pi I}, \tag{16}$$

where I denotes the total nuclear spin. Thus, for an even number of nucleons

$$r = +1(\alpha = 0), \qquad I = 0, 2, 4, \cdots \tag{17}$$

$$r = -1(\alpha = 1), \qquad I = 1, 3, 5, \cdots \tag{18}$$

For an odd number of nucleons

$$r = -\mathrm{i}(\alpha = +\frac{1}{2}), \qquad I = \frac{1}{2}, \frac{5}{2}, \frac{9}{2}, \cdots \tag{19}$$

$$r = +\mathrm{i}(\alpha = -\frac{1}{2}), \qquad I = \frac{3}{2}, \frac{7}{2}, \frac{11}{2}, \cdots \tag{20}$$

Consequently, signature symmetry divides a rotational sequence into two families of levels that differ by $2\hbar$ in spin. The two families share the same intrinsic configuration but have different eigenvalues r. The signature exponent α, defined by $I \equiv \alpha \pmod 2$, labels these families. For an odd particle in an orbital with angular momentum j, the favored signature is

$$\alpha_f = \frac{1}{2}(-1)^{j-\frac{1}{2}}, \tag{21}$$

and the unfavored signature is

$$\alpha_u = \frac{1}{2}(-1)^{j+\frac{1}{2}}, \tag{22}$$

where j represents the total angular momentum of the odd particle [33].

III. RESULTS AND DISCUSSION

The odd-even staggering exhibited by these bands reflects the signature dependence of the Coriolis interaction. We quantify it using

$$S(I) = E(I) - [E(I+1) + E(I-1)]/2. \tag{23}$$

Figure 1 shows $S(I)$ for $^{117-127}$Ba. For the $h_{11/2}$ shell, Eqs. (16) and (17) yield the favored sequence $I = 7/2, 11/2, \cdots$ and the unfavored sequence $I = 5/2, 9/2, \cdots$. The alternating values of $S(I)$ reflect the energy difference between these two negative-parity signature partners. The signature splitting gradually increases up to $2I \approx 22$ and then decreases significantly; anomalous splitting (signature inversion) is observed at high spin in ^{117}Ba, ^{123}Ba, and ^{125}Ba. Similar behavior has been observed in the $A \approx 110$, 130, and 190 mass regions [4, 10, 18, 19, 40, 41], including in recent studies [42–46]. Several interpretations of signature splitting and inversion have therefore been proposed.

The proton and neutron single-particle energies as functions of β_2 are illustrated in Fig. 2. Near $\beta_2 = 0.20$, the relevant proton states arise from the low-K [530]1/2 component of the $h_{11/2}$ shell. For $N = 61-71$, the neutron Fermi level traverses the components with $K = 1/2$ to 7/2. The negative-parity bands considered below are based on an odd neutron occupying an orbital derived from the $\nu h_{11/2}$ shell. For an axially symmetric shape, the

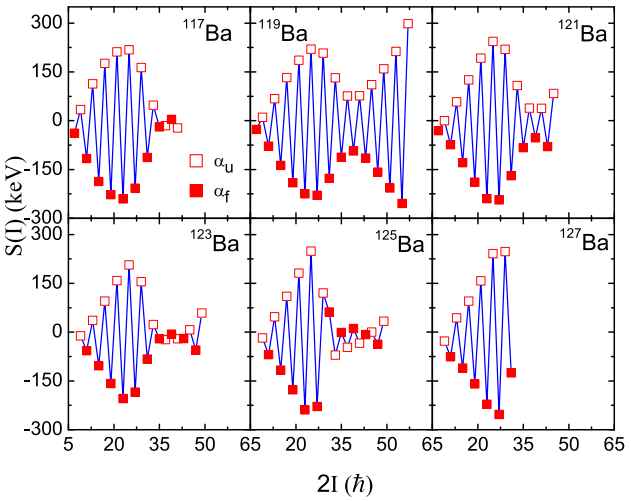


Fig. 1. (color online) Energy-staggering parameter $S(I)$ as a function of $2I$ for $^{117-127}$Ba. Filled and open symbols denote the favored $\alpha_f = -1/2$ and unfavored $\alpha_u = +1/2$ components, respectively, of the $\nu h_{11/2}$ bands. Experimental level energies are taken from ^{117}Ba [34], ^{119}Ba [35], ^{121}Ba [36], ^{123}Ba [37], ^{125}Ba [38], ^{127}Ba [39], respectively.

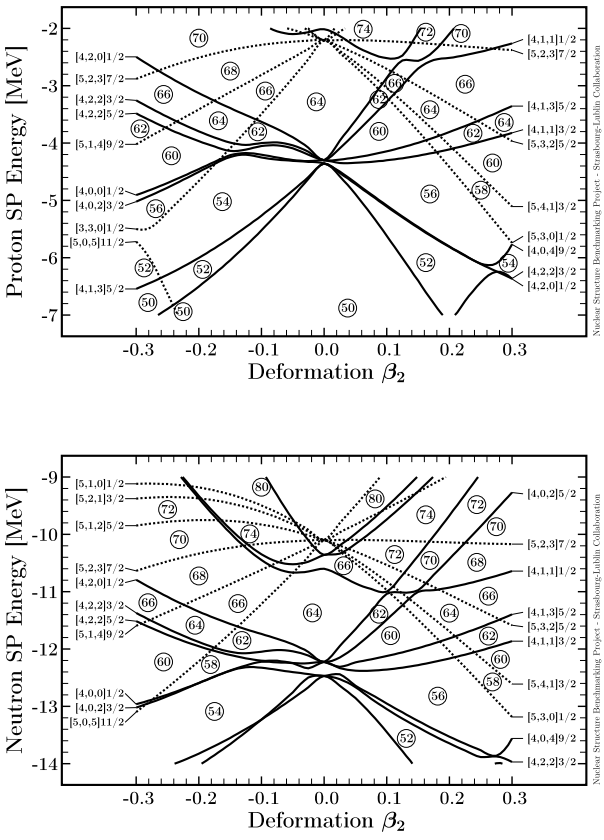


Fig. 2. Proton and neutron single-particle energies as functions of β_2 for ^{130}Ba, calculated with the universal Woods-Saxon Hamiltonian.

Coriolis interaction mixes intrinsic components with different K. Closely spaced components of a unique-parity

shell mix more strongly, and the contribution of low-K components can therefore enhance signature splitting as the rotational frequency increases [6]. In a γ-soft nucleus, the splitting is also sensitive to changes between configurations associated with prolate, triaxial, and oblate minima [18]. Signature splitting in a three-quasineutron rotational band was recently analyzed in Ref. [47].

Figure 3 compares the experimental alignments (solid symbols) with the calculated values (open symbols). The experimental rotational frequency is estimated from

$$\hbar\omega = \frac{E(I+1)-E(I-1)}{I_x(I+1)-I_x(I-1)}, \tag{24}$$

where $I_x = \sqrt{I(I+1)-K^2}$ approximates the angular-momentum component along the rotational x axis; K is the projection on the intrinsic symmetry axis. Panels (a) and (b) show the favored and unfavored signatures, respectively. At low frequency, the neutron contribution includes the angular momentum of the blocked odd quasineutron. Because this odd neutron blocks the alignment of the lowest neutron pair, the first pronounced gain in both signatures of $^{117-125}$Ba is assigned to the alignment of an $h_{11/2}$ proton pair near $\hbar\omega \approx 0.35$ MeV. In ^{127}Ba, the corresponding calculated proton alignment occurs only near 0.60 MeV, and neutron-pair alignment becomes competitive. This result differs from calculations restricted to prolate shapes [23] and from the systematic proton assignment proposed for other proton-rich nuclei near $A \approx 130$ [48].

Equilibrium deformations in soft nuclei can depend appreciably on the model parameters [15]. To examine this dependence across the alignment region, Fig. 4 shows deformation-dependent Routhians at $\hbar\omega = 0.25$, 0.45, and 0.65 MeV. The first frequency lies below the main crossing in the lighter isotopes, whereas the other two sample the post-crossing regime. At $\hbar\omega = 0.25$ MeV, the minima are generally prolate, with $\beta_2 \approx 0.25$, as in the neighboring even-even isotopes $^{118-128}$Ba [15]. With increasing frequency, the β_2 minima in the lighter isotopes remain in the prolate sector, and ^{117}Ba retains a particularly pronounced minimum up to $\hbar\omega = 0.65$ MeV. Toward ^{125,127}Ba, however, the β_2 surfaces become shallower and develop competing minima, indicating increased shape softness after the alignment region.

The evolution in the γ degree of freedom is more pronounced. The lighter isotopes retain minima near the collectively rotating prolate region, whereas the heavier isotopes develop low-lying prolate, triaxial, and oblate alternatives. In particular, an oblate minimum near $\gamma = -60°$ becomes competitive in ^{127}Ba at $\hbar\omega = 0.45$ MeV, and the relative ordering of the shallow minima changes again at $\hbar\omega = 0.65$ MeV. The two signature partners show similar overall β_2 evolution but differ in their γ softness and in the ordering of the competing minima. These changes occur in the frequency region where proton and neutron alignments compete and therefore indicate configuration- and signature-dependent shape competition rather than a universal shape transition [16, 38, 39].

Quasiparticle alignments connect the calculated shape evolution to the observed backbending. As the frequency increases, Routhians belonging to different quasiparticle configurations cross one another. Diabatic trajectories that preserve their wave-function character through these crossings can be associated with the connected experimental rotational bands [2, 49, 50].

Figure 5 shows representative quasiparticle Routhians. Following Ref. [49], lowercase letters label proton orbitals and uppercase letters label neutron orbitals; the negative-parity orbitals are denoted $e, f, \cdots$ and $E, F, \cdots$,

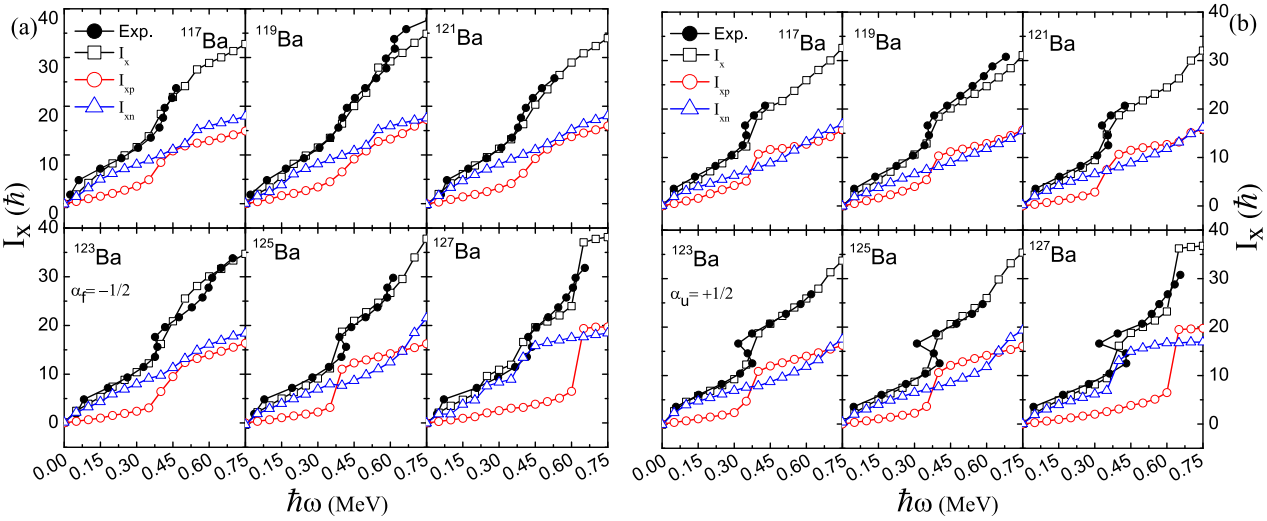


Fig. 3. (color online) Experimental and calculated alignments I_x as functions of $\hbar\omega$ for (a) $\alpha_f = -1/2$ and (b) $\alpha_u = +1/2$. The calculated total alignment and its proton and neutron contributions are shown separately.

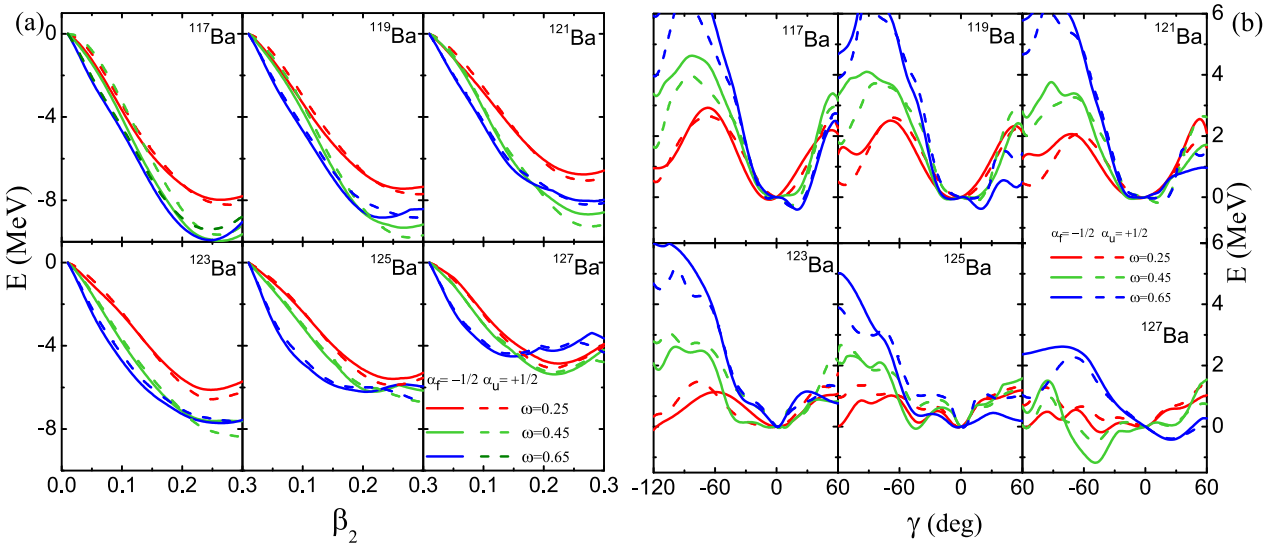


Fig. 4. (color online) Deformation-dependent Routhians for $^{117-127}$Ba as functions of (a) β_2 and (b) γ at $\hbar\omega = 0.25$ (red), 0.45 (green), and 0.65 MeV (blue). (a) Routhians as functions of β_2, minimized with respect to γ and β_4 at each point. (b) Routhians as functions of γ, minimized with respect to β_2 and β_4 at each point. Solid and dashed curves denote $\alpha_f = -1/2$ and $\alpha_u = +1/2$, respectively.

and the positive-parity orbitals are denoted $a, b, \cdots$ and $A, B, \cdots$, respectively. The two-quasiparticle $h_{11/2}$ alignments are labeled ef for protons and EF for neutrons. In Fig. 5, the $\pi(h_{11/2})^2$ and $\nu(h_{11/2})^2$ crossings both occur near $\hbar\omega = 0.35$ MeV. In an odd-N band based on the lowest quasineutron, however, the EF neutron alignment is blocked. Accordingly, the first calculated gain in Fig. 3 is assigned primarily to the $\pi(h_{11/2})^2$ crossing.

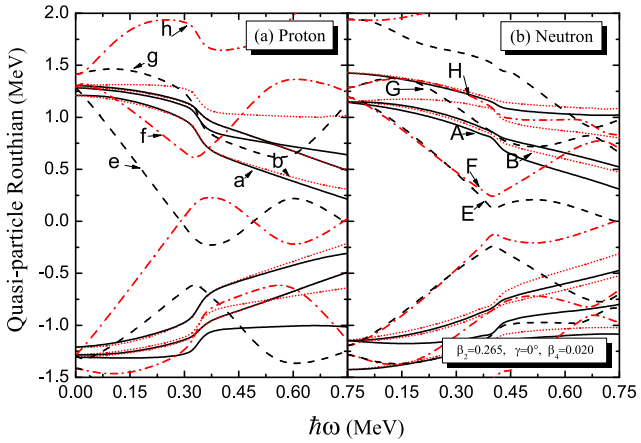


Fig. 5. (color online) Calculated quasiparticle Routhians as functions of $\hbar\omega$ for (a) quasiproton and (b) quasineutron orbitals in ^{121}Ba at $\beta_2 = 0.265$, $\gamma = 0°$, and $\beta_4 = 0.020$. The parity and signature (π, α) of the Routhians are represented as follows: $(+,+1/2)$ solid lines, $(+,-1/2)$ dotted lines, $(-,+1/2)$ dash-dotted lines, and $(-,-1/2)$ dashed lines.

The remainder of the analysis focuses on the lowest E and F quasineutron Routhians associated with the observed $\nu h_{11/2}$ bands. Figure 6 compares the isotopes at the common representative deformation $\beta_2 = 0.265$, $\gamma = 0°$, and $\beta_4 = 0.020$. The vertical marker at $\hbar\omega = 0.250$ MeV lies below the proton crossing.

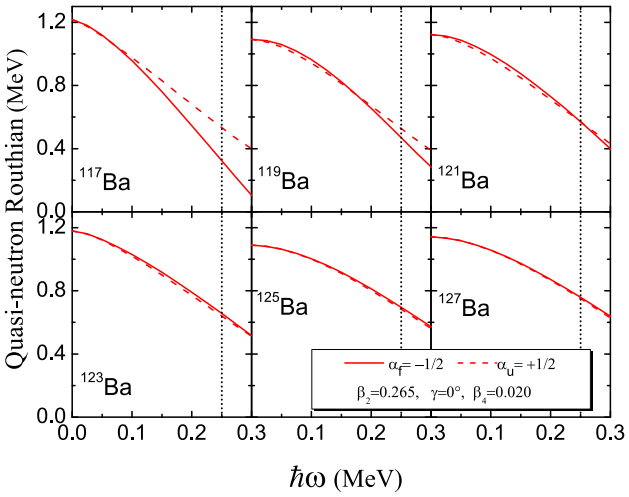


Fig. 6. (color online) Lowest $h_{11/2}$ quasineutron Routhians E and F as functions of $\hbar\omega$ for $^{117-127}$Ba at $\beta_2 = 0.265$, $\gamma = 0°$, and $\beta_4 = 0.020$. Solid and dashed curves denote $\alpha_f = -1/2$ (E) and $\alpha_u = +1/2$ (F), respectively. The vertical dotted lines mark $\hbar\omega = 0.250$ MeV.

At zero rotational frequency, the two signature partners are degenerate. As $\hbar\omega$ increases, the E and F trajectories separate most visibly in the lighter isotopes, particularly in ^{117}Ba, whereas they remain close or cross in the heavier isotopes. At the reference frequency $\hbar\omega = 0.250$

MeV, the magnitude of the calculated E–F splitting decreases overall from $N = 61$ to $N = 71$. This trend reflects the migration of the neutron Fermi level from low-K toward higher-K components of the $h_{11/2}$ shell. Because all six panels use the same axial deformation, Fig. 6 isolates the neutron-number dependence of the underlying single-particle structure. The additional sensitivity to the equilibrium deformation is examined next.

Since signature splitting is sensitive to deformation [3, 13, 18, 19], a change across the crossing may indicate different equilibrium shapes for the one- and three-quasiparticle configurations. Figure 7 separates the β_2 and γ dependences at $\hbar\omega = 0.250$ MeV. In Fig. 7(a), the splitting is small at large prolate deformation but increases rapidly as β_2 decreases. At small β_2, it also tends to decrease with increasing neutron number. This trend is consistent with stronger Coriolis mixing when the relevant $h_{11/2}$ components are closely spaced [3]. At the equilibrium β_2 values indicated in the insets, the calculated splitting is small throughout the isotope chain. Thus, within this calculation, variations in β_2 near the equilibrium values are not the principal source of the observed isotope-dependent staggering.

We therefore use $\beta_2 = 0.250$ as a common reference value to isolate the γ dependence in Fig. 7(b). At fixed $\hbar\omega$ and β_2, Fig. 7(b) shows that the two signatures have different γ-driving tendencies. With increasing neutron number, the minimum of the favored E Routhian moves from negative γ toward the collective oblate limit at $\gamma = -60°$, whereas the unfavored F Routhian evolves from positive-γ triaxiality toward an oblate minimum.

This evolution reflects the combined action of Coriolis and nonaxial quadrupole couplings. The former, $\langle j,\Omega = \pm 1/2|j_1|j,\Omega = \mp 1/2\rangle$, mixes the signature partners through their $\Omega = 1/2$ components and dominates near prolate shapes when the Fermi level lies among low-K orbitals. As the shape becomes triaxial, the latter, $\langle j,\Omega = \pm 1/2|Y_{22} + Y_{2-2}|j,\Omega = \mp 3/2\rangle$, mixes the $\Omega = 1/2$ and $3/2$ components and can alter the signature ordering [33]. Since both couplings enter coherently in the diagonalization, they cannot be assigned unique additive contributions.

Whether the ordering reverses therefore depends on the position of the neutron Fermi level. In ^{117}Ba, its low-K position allows the Coriolis contribution to preserve the same favored signature from the near-prolate to the collective-oblate region. In $^{123-127}$Ba, the higher-K character makes the splitting small without a clear reversal. Only in ^{119,121}Ba is the Fermi level intermediate, so the increasing nonaxial mixing can overcome the near-prolate ordering and interchange the E and F Routhians. This interpretation is consistent with the low-K to high-K migration discussed for Fig. 6. Because β_4 varies only weakly, the sensitivity calculations use the common value $\beta_4 = 0.020$.

Because the proton Fermi surface lies in the lower part of the intruder shell, near the low-K components of $h_{11/2}$, the lowest quasiproton Routhians are expected to exhibit stronger signature splitting. Figure 8 shows its dependence on $\hbar\omega$, β_2, and γ. In particular, the slopes in panel (c) indicate that the quasiproton favors positive γ. The calculated e–f separation reaches approximately 0.8 MeV, much larger than the E–F separation at the same representative deformation. A strong signature dependence of low-K quasiproton Routhians has also been found in neighboring odd-odd nuclei [4, 18, 19, 41, 51, 52]. After proton-pair alignment, the positive-γ tendency of the proton orbitals competes with the negative-γ tendency of the odd neutron. This partial cancellation shifts

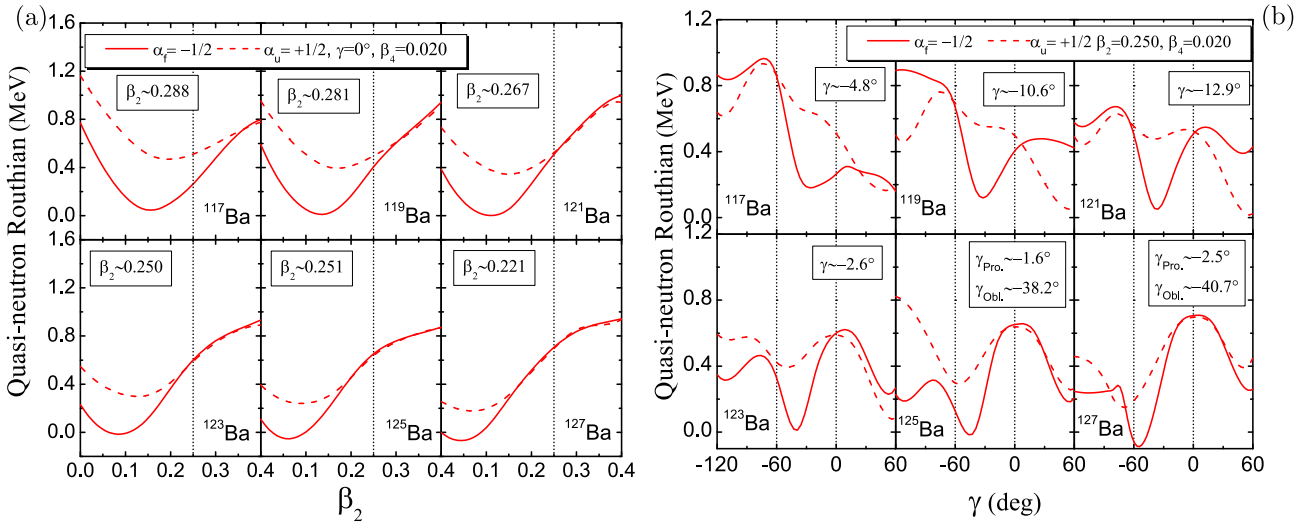


Fig. 7. (color online) Lowest $h_{11/2}$ quasineutron Routhians E and F in $^{117-127}$Ba at $\hbar\omega = 0.250$ MeV as functions of (a) β_2, with $\gamma = 0°$ and $\beta_4 = 0.020$, and (b) γ, with $\beta_2 = 0.250$ and $\beta_4 = 0.020$. Insets give the corresponding TRS equilibrium deformations. Solid and dashed curves denote $\alpha_f = -1/2$ (E) and $\alpha_u = +1/2$ (F), respectively.

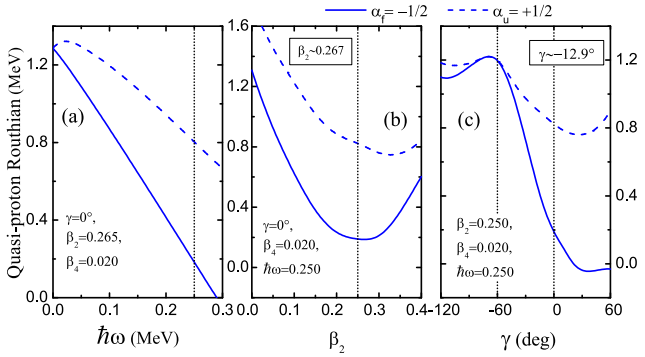


Fig. 8. (color online) Lowest $h_{11/2}$ quasiproton Routhians e and f in ^{121}Ba as functions of (a) $\hbar\omega$, (b) β_2, and (c) γ. The fixed deformation parameters are the same as those used in Figs. 6 and 7. Solid and dashed blue curves denote $\alpha_f = -1/2$ (e) and $\alpha_u = +1/2$ (f), respectively.

the equilibrium shape closer to $\gamma = 0°$ and provides a qualitative mechanism for the reduced experimental splitting in Fig. 1.

Figure 9 tests this interpretation above the first crossing. At the equilibrium β_2 values shown in Fig. 9(a), the post-crossing splitting remains small in $^{117-121}$Ba and is nearly zero in $^{123-127}$Ba. Panel (b) shows the corresponding γ dependence. In ^{117}Ba, the splitting passes through zero near $\gamma \approx +10°$, as does the calculated splitting in ^{123}Ba. For ^{119,121}Ba, the finite separation at the equilibrium minima is consistent with an increase above the crossing. The heavier isotopes again display competing minima with different signature dependence.

The changes in ordering occur in each of the three Lund sectors, $-120° < \gamma < -60°$, $-60° < \gamma < 0°$, and $0° < \gamma < 60°$, which correspond to rotation about the long, medium, and short principal axes, respectively [16]. A similar dependence was found for odd-odd nuclei near $A \approx 130$ [53]. Quadrupole pairing can also modify signature splitting in odd-odd systems [6]; its role in the present odd-A nuclei is not included and remains a source of model uncertainty.

In neighboring even-even Ba nuclei, two positive-parity bands have been observed in addition to the ground-state band. These bands have nearly the same energy and are attributed to the alignment of two $h_{11/2}$ protons in one case and two $h_{11/2}$ neutrons in the other. This behavior arises from shape changes induced by the aligned quasiparticles. Specifically, the alignment of two high-K $h_{11/2}$ neutrons tends to drive the nucleus toward an oblate shape, while adding one neutron in a $\nu h_{11/2}$ orbital outside the even-even core can stabilize a triaxial deformation, as discussed in Refs. [14–16, 48].

The results for ^{125,127}Ba are consistent with the behavior calculated for the neighboring even-even nucleus ^{126}Ba: in both cases, prolate and triaxial or oblate minima coexist [15, 16]. In an odd-A nucleus, blocking makes the crossing pattern configuration- and signature-dependent. Because the two heavier isotopes exhibit similar shape competition, Fig. 10 uses ^{125}Ba as a representative example.

Figure 10(a) compares the measured alignment with calculations for the two competing shapes. The calculated backbending is dominated by proton alignment in the prolate minimum and by neutron alignment in the triaxial-oblate minimum for both signatures. Figure 10(b) identifies the crossings. Because the EF neutron alignment is blocked, the first crossing must involve either the first unblocked neutron pair (FG or EH, depending on signature) or the proton pair ef. The E band can therefore be crossed by Eef or EFG, and the F band by Fef or FEH.

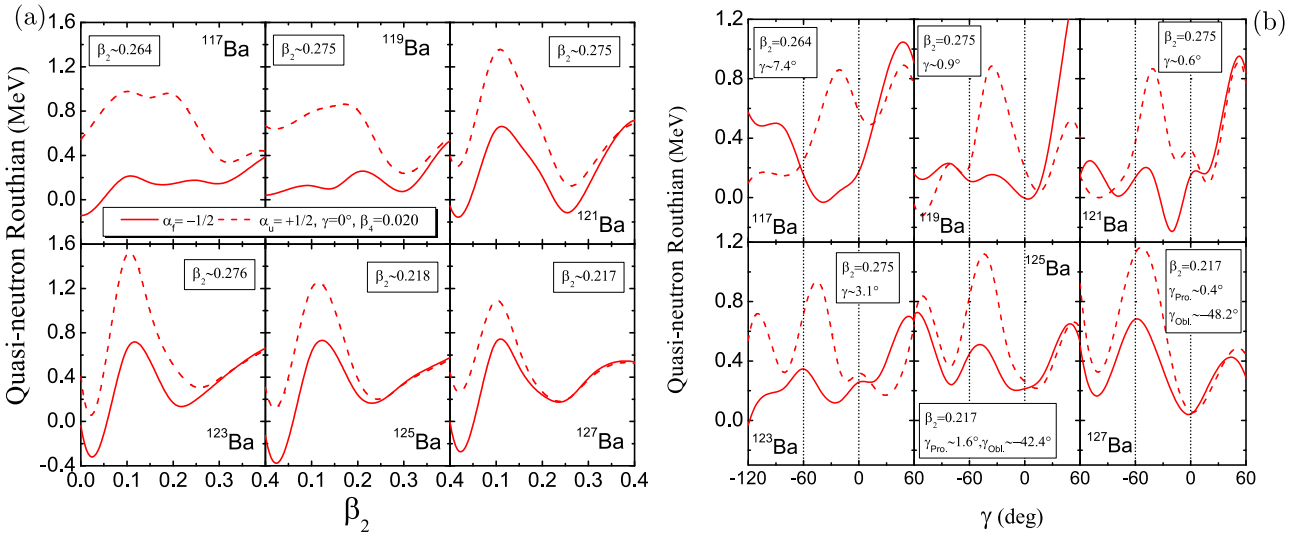


Fig. 9. (color online) Same as Fig. 7, but at $\hbar\omega = 0.45$ MeV, above the first crossing in the lighter isotopes. Insets show the TRS equilibrium deformations. Solid and dashed curves denote $\alpha_f = -1/2$ (E) and $\alpha_u = +1/2$ (F), respectively.

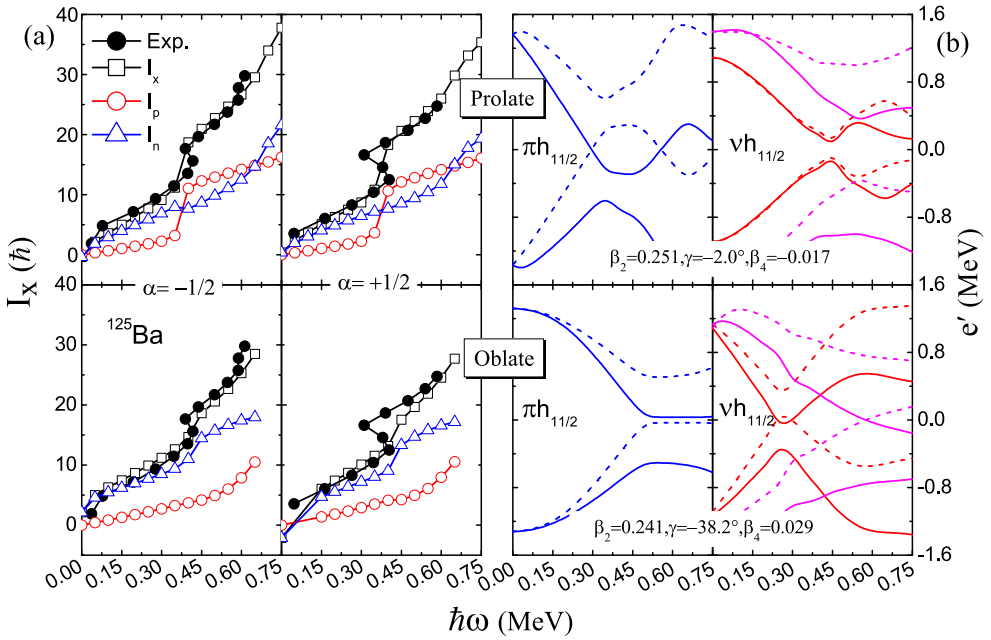


Fig. 10. (color online) Results for ^{125}Ba. (a) Experimental total alignments (solid black circles) and calculated total alignments I_x (open symbols), together with the proton (I_p) and neutron (I_n) contributions for both signatures. (b) Calculated quasiparticle Routhians: proton ef (blue), neutron EF (red), and neutron GH (magenta). The upper panels use the prolate configuration $(\beta_2,\gamma,\beta_4) = (0.251,-2.0^\circ,0.020)$; the lower panels use the triaxial-oblate configuration $(0.241,-38.2^\circ,0.021)$.

In the figure, the lowest quasiproton ef bands of $\pi h_{11/2}$ are shown in blue, the lowest quasineutron EF bands are in red, and the first negative signature partner bands GH are in magenta. Solid curves represent the favored signature $\alpha_f = -1/2$, while dashed curves indicate the unfavored signature $\alpha_u = +1/2$. For the prolate deformation, the proton ef crossing occurs near $\hbar\omega \approx 0.35$ MeV, whereas the neutron FG crossing lies above 0.55 MeV. The resulting three-quasiparticle configurations are Eef for the favored signature and Fef for the unfavored signature. For the triaxial-oblate deformation, the proton crossing moves to about 0.50 MeV, while the neutron FG/EH crossings occur near 0.37 MeV and produce EFG and FEH, respectively. Thus the G and H quasineutron orbitals control both the first alignment and much of the post-crossing signature dependence in this minimum. In the prolate minimum, the post-crossing bands are dominated by Eef and Fef; once the proton pair is aligned, their relative behavior reflects the E and F quasineutron Routhians. In the triaxial-oblate minimum, the splitting instead follows the G and H Routhians.

Figure 11 therefore compares the EF and GH quasineutron Routhians as functions of γ at $\hbar\omega = 0.45$ MeV for ^{125}Ba and ^{127}Ba. The insets show the experimental staggering for the bands assigned to the competing shapes. The G and H quasineutron Routhians become energetically competitive above the first alignment. The EF splitting remains small, whereas the GH splitting is pronounced in both nuclei. The GH minima move toward the collective-oblate limit ($\gamma = -60^\circ$), while the EF minima remain near prolate. The calculation therefore associates neutron-pair alignment with a transition toward a collectively rotating oblate shape, consistent with the alignment trend in Fig. 3(b). At prolate deformation, by contrast, the EF splitting is small or inverted. The relevant experimental partners are bands (7) and (8) in ^{125}Ba [38] and bands (5) and (6) in ^{127}Ba [39], particularly near $I = 29/2$ and $31/2$. In the prolate bands of ^{125,127}Ba, the renewed increase in splitting at high spin accompanies the second upbending. For ^{125}Ba, the calculated FG/EH neutron crossing gives the five-quasiparticle configurations $EefFG$ ($\alpha = -1/2$) and $FefEH$ ($\alpha = +1/2$) [3]. For ^{127}Ba, the corresponding assignments are $EFGef$ and $FEHef$ [39]. No comparable reduction or inversion is established for the bands assigned to the triaxial-oblate minimum: band (4) in ^{125}Ba [38] and band (15) in ^{127}Ba [39]. The large calculated G–H separation offers a possible, but not unique, explanation for why a high-spin signature partner has not been identified experimentally.

The calculations thus suggest two high-spin structures in nuclei with shape coexistence: a pair of prolate signature partners and a triaxial-oblate band for which only one signature may be observed. Similar spectra occur in neighboring odd-A nuclei [48]. Figure 12 extends the comparison to Ba, Ce, and Nd isotopes, separating bands assigned to proton and neutron alignments. This separation leads to a different systematics of the staggering from analyses that combine the bands without regard to the aligned configuration [23, 48, 54].

As shown in Figure 12, for $N = 67-75$, the available

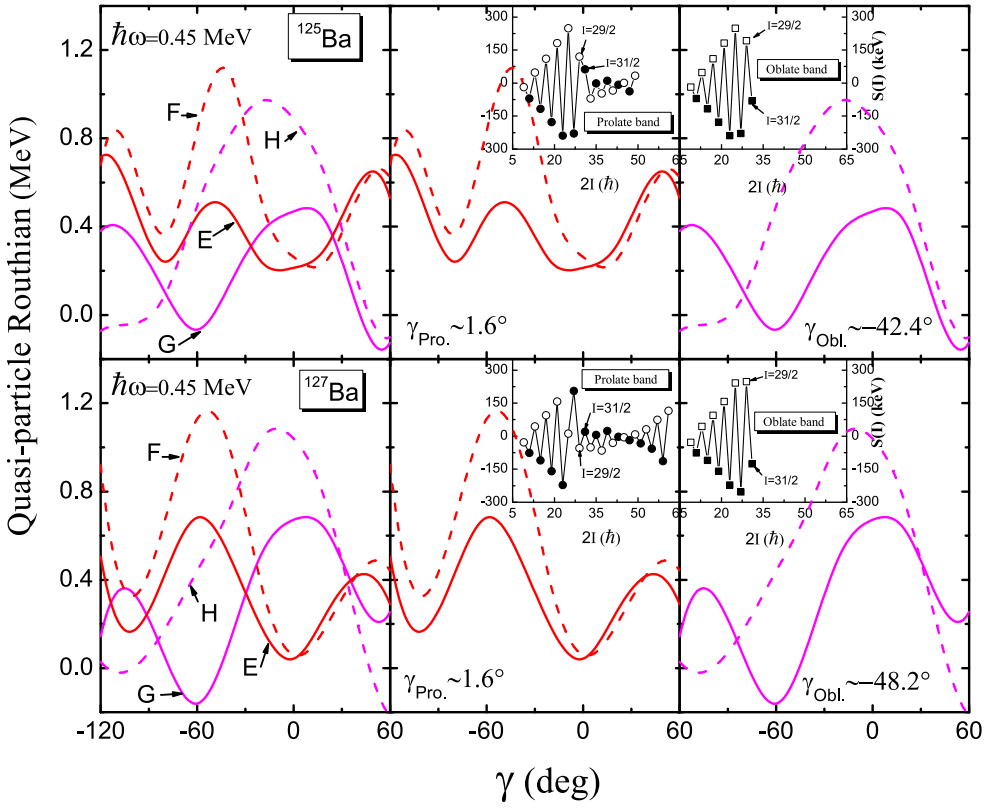


Fig. 11. (color online) Quasineutron EF and GH Routhians as functions of γ for ^{125}Ba and ^{127}Ba at $\hbar\omega = 0.45$ MeV, with $\beta_2 = 0.217$ and $\beta_4 = 0.020$. Insets show the experimental energy-staggering parameter $S(I)$ for the bands assigned to the prolate and triaxial-oblate minima.

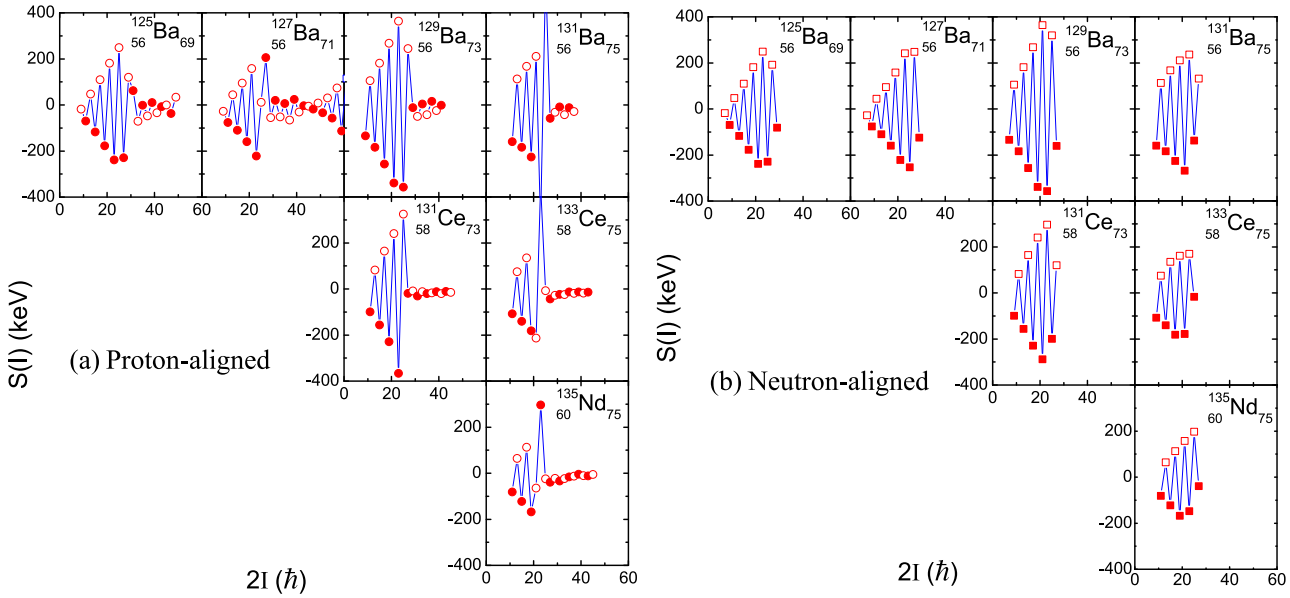


Fig. 12. (color online) Experimental $S(I)$ values for $h_{11/2}$ bands in odd-A Ba ($Z = 56$), Ce ($Z = 58$), and Nd ($Z = 60$) isotopes. Filled and open symbols denote the favored $\alpha_f = -1/2$ and unfavored $\alpha_u = +1/2$ signatures, respectively. The adopted bandheads have $K = 7/2$ for $N = 67$–71 and $K = 9/2$ for $N = 73$–75. Circles in (a) denote proton-aligned bands; squares in (b) denote neutron-aligned bands. Experimental data are taken from ^{129}Ba [54], ^{131}Ba [55], ^{131}Ce [56], ^{133}Ce [57], and ^{135}Nd [58].

systematics favor triaxial or oblate ground-state shapes [48], and neutron alignment can compete in the yrast sequence. The combined data support the same qualitative pattern as the TRS results: the prolate configuration tends

to appear as a pair of bands with reduced or inverted splitting, whereas the triaxial-oblate configuration often appears as a single high-spin band. These systematics support the interpretation that proton and neutron alignments influence both shape coexistence and the observed signature splitting. They do not, by themselves, uniquely determine the shape; the assignment relies on the combined alignment and Routhian analysis above.

IV. SUMMARY

We have analyzed signature splitting in the $\nu h_{11/2}$ bands of the odd-N isotopes $^{117-127}$Ba. The experimental staggering parameter $S(I)$ generally increases toward $2I \approx 22$ and then decreases; in several isotopes the ordering of the signatures reverses at higher spin.

Pairing- and deformation-self-consistent Woods-Saxon-Strutinsky calculations were used to connect this behavior to quasiparticle alignment and shape evolution in (β_2,γ,β_4) space. The first calculated alignment in $^{117-123}$Ba is dominated by an $h_{11/2}$ proton pair. In ^{125,127}Ba, proton and neutron alignmentscompete because the alignment frequencies depend strongly on the prolate and triaxial-oblate minima.

Sensitivity studies of the lowest quasineutron Routhians show that changes of β_2 near the equilibrium values produce only a small splitting, whereas the ordering and separation of the signatures vary strongly with γ. The reduction or inversion after proton alignment can therefore be understood qualitatively as a competition between the negative-γ tendency of the strongly coupled odd neutron and the positive-γ tendency of the aligned proton pair.

For the heavier isotopes, the first unblocked neutron crossing (FG/EH) is favored in the triaxial-oblate minimum and produces a large G–H separation. This offers a possible explanation for the absence of an observed high-spin partner, while the smaller or inverted splitting of the prolate bands is consistent with $\pi(h_{11/2})^2$ alignment. The assignments remain model dependent, but the combined isotope, alignment, and deformation systematics provide a coherent interpretation of the observed splitting.

References

[1] A. Bohr and B. R. Mottelson, *Nuclear Structure, Vol. II: Nuclear Deformations* (New York: W. A. Benjamin, 1975).
[2] M. J. A. De Voigt, J. Dudek, Z.Szymański, Rev. Mod. Phys. **55**(4), 949 (1983)
[3] A. Granderath, P.E Mantica, R. Bengtsson *et al*., Nucl. Phys. A **597**, 427 (1996)
[4] W. F. Mueller, H. J. Jensen, W. Reviol *et al*., Phys. Rev. C **50**(4), 1901 (1994)
[5] I. Hamamoto, Phys. Lett. B **235**, 221 (1990)
[6] F. R. Xu, W. Satuła, R. Wyss, Nucl. Phys. A **669**, 119 (2000)
[7] F. S. Stephens, Rev. Mod. Phys. **47**, 43 (1975)
[8] J. Meyer-ter-Vehn, Nucl. Phys. **A249**, 111 (1975)
[9] R. Aryaeinejad, D. J. G Love, A. H. Nelson *et al*., J. Phys. G: Nucl. Phys. **10**, 955 (1984)
[10] A. Ikeda and T. Shimano, Phys. Rev. C **42**, 149 (1990)
[11] M. Matsuzaki, Phys. Rev. C **46**, 1548 (1992)
[12] P. B. Semmes and I. Ragnarsson, AIP Conference Proceedings **259**, 566 (1992)
[13] R. Bengtsson, H. Frisk, FR. May, J. A. Pinston, Nucl. Phys. A **415**, 189 (1984)
[14] R. Wyss, A. Granderath, R. Bengtsson *et al*., Nucl. Phys. A **505**, 337 (1989)
[15] J. Yang, H. L. Wang, and M. L. Liu, Prog. Theor. Exp. Phys. **2016**(6), 063D (2016)
[16] J. Yang, X. Guan, R. X. Nie *et al*., Chin. Phys. C **49**(7), 074104 (2025)
[17] Y. Liang, R. Ma, E. S. Paul *et al*., Phys. Rev. C **42**(3), 890 (1990)
[18] S. Frauendorf and F. R. May, Phys. Lett. B **125**, 245 (1983)
[19] Y. S. Chen, S. Frauendorf and G.A. Leander, Phys. Rev. C **28**, 2437 (1983)
[20] P. W. Zhao, S. Q. Zhang, and J. Meng, Phys. Rev. C **92**(3), 034319 (2015)
[21] M. A. Cunningham, Nucl. Phys. A **385**, 204 (1982)
[22] A. Gizon, B. Weiss, P. Paris *et al*., Eur. Phys. J. **A8**, 41 (2000)
[23] A. Bharti, S. Singh and S. K. Khosa, Int. J. of Mod. Phys. E **20**(05), 1183 (2011)
[24] W. Satuła, R. Wyss, and P. Magierski, Nucl. Phys. A, **578**, 45 (1994)
[25] W. D. Myers, W. J. Swiatecki, Nucl. Phys. **81**, 1 (1966)
[26] V. M. Strutinsky, Nucl. Phys. A, **95**, 420 (1967)
[27] H. J. Lipkin, Ann. Phys. **9**, 272 (1960)
[28] Y. Nogami, Phys. Rev. **134**, B313 (1964)
[29] P. Möller and J. R. Nix, Nucl. Phys. A, **536**, 20 (1992)
[30] C. Ćwiok, J. Dudek, W. Nazarewicz *et al*, Comp. Phys. Comm. **46**, 379 (1987)
[31] W. Nazarewicz, J. Dudek, R. Bengtsson *et al*, Nucl. Phys. A, **435**, 397 (1985)
[32] G. Andersson, S. E. Larsson, G. Leander *et al*, Nucl. Phys. A, **268**, 205 (1976)
[33] I. Hamamoto, Nucl. Phys. A, **520**, 297 (1990)
[34] B. Ding, Z. Liu, D. Seweryniak *et al*., Phys. Rev. C **95**, 024301 (2016)
[35] J. F. Smith, C. J. Chiara, D. B. Fossan *et al*., Phys. Rev. C **61**(4), 044329 (2000)
[36] F. Lidtén, L. Hildingsson, T. Lindblad *et al*., Nucl. Phys. A **524**, 141 (1991)
[37] R. Wyss, F. Lidén, J. Nyberg *et al*., Z. Phys. A - Atomic Nuclei **330**, 123 (1988)
[38] D. Ward, AIP Conference Proceedings **259**, 358 (1992)
[39] A. Dewald, A. Schmidt, G. Alexius *et al*., Eur. Phys. J. A **3**, 103 (1998)
[40] C. Liu, S. Y. Wang, B. Qi *et al*., Phys. Rev. C **88**, 037301 (2013)
[41] J. Kownacki, J. D. Garrett, J. J. GaardhØje *et al*., Nucl. Phys. A **394**, 269 (1983)
[42] N. Kumar, S. Kumar, S. K. Mandal *et al*, Eur. Phys. J. A **53**, 25 (2017)

[43] B. Das, P. Datta, S. Chattopadhyay *et al*, Phys. Rev. C **98**, 014326 (2018)
[44] B. Das, N. Rather, P. Datta *et al*, Phys. Rev. C **95**, 051301 (2017)
[45] W. J. Sun and J. Li, Chin. Phys. C **43**, 094104 (2019)
[46] B. Ding, C. M. Petrache, S. Guo *et al*, Phys. Rev. C **104**, 064304 (2021)
[47] M. Kaur, S. Kumar, S. Singh and A. K. Jain, Chin. Phys. C **49**(10), 104103 (2025)
[48] O. Zeidan, D. J. Hartley, L. L. Riedinger *et al*, Phys. Rev. C **65**, 024303 (2002)
[49] R. Bengtsson and S. Frauendorf, Nucl. Phys. A **327**, 139 (1979)
[50] R. Bengtsson and J. D. Garrett, *The cranking model-theoretical and experimental bases* Collective phenomena in atomic nuclei. (1984).
[51] D. J. Hartley, A. Galindo-Uribarri, C. Baktash *et al*, Phys. Rev. C **63**, 041301 (2001)
[52] C. H. Yu, M. A. Riley, J. D. Garrett *et al*., Nucl. Phys. A **489**, 477 (1988)
[53] Z. C. Gao, Y. S. Chen, and Yang Sun, Phys. Lett. B **634**, 195 (2006)
[54] A. P. Byrne, K. Schiffer, G. D. Dracoulis *et al*., Nucl. Phys. A **548**, 131 (1992)
[55] N. Kaur, A. Kumar, G. Mukherjee *et al*., Eur. Phys. J. A **50**, 5 (2014)
[56] M. Palacz, Z. Sujkowski, J. Nyberg *et al*., Z. Phys. A **338**, 467 (1991)
[57] K. Hauschild, R. Wadsworth, R. M. Clark *et al*., Phys. Rev. C **54**, 613 (1996)
[58] W. F. Piel, Jr. C. W. Beausang, D. B. Fossan *et al*., Phys. Rev. C **35**, 959 (1987)